STAT3 activation of SCAP-SREBP-1 signaling upregulates fatty acid synthesis to promote tumor growth

Yunzhou Fan, Rui Zhang, Chao Wang, Meixia Pan, Feng Geng, Yaogang Zhong, Huali Su, Yongjun Kou, Xiaokui Mo, Etienne Lefai, et al.

STAT3 activation of SCAP-SREBP-1 signaling upregulates fatty acid synthesis to promote tumor growth

Received for publication, January 27, 2024, and in revised form, April 23, 2024 Published, Papers in Press, May 6, 2024,
https://doi.org/10.1016/j.jbc.2024.107351

Yunzhou Fan[1,2], Rui Zhang[1], Chao Wang[1], Meixia Pan[3], Feng Geng[1,2], Yaogang Zhong[1,2], Huali Su[1,2], Yongjun Kou[1,2], Xiaokui Mo[4], Etienne Lefai[5], Xianlin Han[3], Arnab Chakravarti[1], and Deliang Guo[1,2,*]

From the [1]Department of Radiation Oncology, Ohio State Comprehensive Cancer Center, Arthur G. James Cancer Hospital and Richard J. Solove Research Institute, and College of Medicine at The Ohio State University, Columbus, Ohio, USA; [2]Center for Cancer Metabolism, James Comprehensive Cancer Center at The Ohio State University, Columbus, Ohio, USA; [3]Barshop Institute for Longevity and Aging Studies, and Department of Medicine, University of Texas Health Science Center at San Antonio, San Antonio, Texas, USA; [4]Biostatistic Center and Department of Bioinformatics, College of Medicine at The Ohio State University, Columbus, Ohio, USA; [5]Human Nutrition Unit, French National Research Institute for Agriculture, Food and Environment, University Clermont Auvergne, Clermont-Ferrand, France

Reviewed by members of the JBC Editorial Board. Edited by George M. Carman

SCAP plays a central role in controlling lipid homeostasis by activating SREBP-1, a master transcription factor in controlling fatty acid (FA) synthesis. However, how SCAP expression is regulated in human cancer cells remains unknown. Here, we revealed that STAT3 binds to the promoter of *SCAP* to activate its expression across multiple cancer cell types. Moreover, we identified that STAT3 also concurrently interacts with the promoter of *SREBF1* gene (encoding SREBP-1), amplifying its expression. This dual action by STAT3 collaboratively heightens FA synthesis. Pharmacological inhibition of STAT3 significantly reduces the levels of unsaturated FAs and phospholipids bearing unsaturated FA chains by reducing the SCAP-SREBP-1 signaling axis and its downstream effector SCD1. Examination of clinical samples from patients with glioblastoma, the most lethal brain tumor, demonstrates a substantial co-expression of STAT3, SCAP, SREBP-1, and SCD1. These findings unveil STAT3 directly regulates the expression of SCAP and SREBP-1 to promote FA synthesis, ultimately fueling tumor progression.

Rapidly dividing tumor cells require a continuous supply of fatty acids (FAs) to generate sufficient phospholipids for membrane biogenesis (1, 2). FA synthesis is known to be upregulated in various cancers to meet this demand (2–5). *De novo* FA synthesis begins with the production of palmitic acid, consisting of 16 saturated carbons (C16:0), and is generated by fatty acid synthase (FASN) (1). Palmitic acid undergoes a sequential process of desaturation and elongation, resulting in the formation of several new FAs, including palmitoleic acid (C16:1), stearic acid (C18:0) and oleic acid (C18:1) (6–8). Within this process, stearoyl-CoA desaturase 1 (SCD1) converts palmitic acid and stearic acid into monounsaturated palmitoleic acid and oleic acid (6–8). Numerous studies have highlighted the critical role of oleic acid in supporting tumor growth (9–11). It can prevent saturated palmitic acid-induced endoplasmic reticulum (ER) stress (12, 13) and neutralize polyunsaturated FA levels to prevent peroxidation and the initiation of ferroptosis (14). Thus, high levels of SCD1 ensure an ample supply of oleic acid to sustain tumor growth (1). In contrast, the role of palmitoleic acid in cancer growth has been less studied (15, 16).

The *de novo* FA synthesis pathway is under the control of sterol regulatory element-binding protein 1 (SREBP-1), the master transcription factor of lipogenesis, which regulates the expression of both *FASN* and *SCD1* (1, 17, 18). We previously demonstrated that the high upregulation of SREBP-1 in glioblastoma (GBM), the most lethal type of primary brain tumor (19, 20) and in lung cancer, promotes the expression of *FASN* and *SCD1* to support rapid tumor growth (21). The elevated expression of SREBP-1 has subsequently been validated in various other cancer types, including liver, pancreatic, breast, and melanoma (3, 21–23).

The family of SREBPs comprises three members: SREBP-1a, -1c, and -2, collectively controlling the expression of genes in regulating fatty acid and cholesterol synthesis (1, 18, 24). Specifically, SREBP-1c primarily mediates fatty acid synthesis, SREBP-2 mediates cholesterol synthesis and SREBP-1a regulates both processes (6, 24). SREBPs are initially synthesized as inactive precursors localized in the ER membrane. They require SREBP cleavage-activation protein (SCAP) to transport them from the ER to the Golgi for sequential cleavage. This process releases the N-terminal active SREBP isoforms, allowing them to enter the nucleus and activate the expression of lipogenic genes (3, 17, 18, 21, 25, 26). Previous research has mainly focused on the regulation of SCAP-SREBP translocation, including cholesterol-mediated feedback inhibition (17, 24), as well as glucose, glutamine, and ammonia-activated trafficking (1–3, 18, 21). Our group has demonstrated that genetic inhibition or mutation of *SCAP* significantly suppresses tumor growth in GBM and lung cancer orthotopic mouse models, highlighting SCAP as a promising molecular

* For correspondence: Deliang Guo, deliang.guo@osumc.edu.

target for cancer treatment (3, 21). However, how SCAP is upregulated in human cancers to promote SREBP-1 activation, and FA synthesis is unknown. Understanding this process could contribute to the development of effective approaches for targeting various types of cancer.

Signal transducer and activator of transcription 3 (STAT3), an oncogenic transcription factor implicated in tumorigenesis, exhibit hyperactivation in various cancer types, including brain, lung, liver, breast, colon, and prostate cancers. This hyperactivation can be induced by multiple factors, such as growth factors, oncogenic proteins, carcinogens, and cytokines (27–30). STAT3 is typically activated through phosphorylation at tyrosine 705 (Try705), which leads to dimerization and nuclear translocation. Consequently, STAT3 regulates the transcription of various pro-tumoral genes, including *CCND1* (encoding *cyclin D1*), *c-myc*, *Survivin,* and *VEGF*, collectively promoting tumor progression (31, 32). Targeting STAT3 using small-molecule inhibitors, such as napabucasin (Napa), or degraders has been extensively tested in preclinical xenograft models and in Phase II/III clinical trials for various cancer therapy, including GBM, lung, liver, gastrointestinal, colorectal, and pancreatic cancers (32–35).

In this study, we observed that pharmacological inhibition of STAT3 by Napa in GBM cells led to a significant reduction in palmitoleic acid, oleic acid and other unsaturated FA levels. This was accompanied by a notable alteration in phospholipid profiles. Further investigation revealed that STAT3 directly binds to the promoters of *SCAP* and *SREBF1* (which encodes for SREBP-1) to activate their expression. This, in turn, upregulates the SCAP-SREBP-1-FASN-SCD1 axis, increasing *de novo* FA synthesis and desaturation and consequently promoting tumor growth.

Results

Inhibition of STAT3 significantly reduces free FA levels and disrupts phospholipid homeostasis in GBM cells

To investigate whether STAT3 plays a role in regulating FA synthesis and phospholipid formation in cancer cells, we conducted lipidomics analysis on GBM U251 cells treated with Napa, a well-studied STAT3 inhibitor that has been used in Phase II/III clinical trials for various cancers (Fig. 1*A*) (32, 36, 37). This treatment induced significant changes in the lipid profiles of the GBM cells (Fig. 1, *B*–*I*). Notably, various species of phosphatidic acid (PA), phosphatidylinositol (PI), phosphatidylserine (PS), and sphingomyelin (SM) were significantly reduced following Napa treatment as compared to untreated cells (Fig. 1, *D*–*G*). Additionally, multiple species of phosphatidylcholine (PC), phosphatidylethanolamine (PE), lysophosphatidylcholine (LPC), and SM exhibited alterations, with some increasing and others decreasing compared to control cells (Fig. 1*H*). Upon closer examination of the altered lipid species, it became evident that most of the decreased phospholipids contained unsaturated fatty acid chains (Fig. 1, *D*–*H*). Further analysis of free FA (FFA) levels in GBM cells revealed that Napa treatment significantly reduced the levels of many FAs, particularly for mono- and polyunsaturated FAs, including C16:1, C16:2, C18:1, C18:2, C20:1, C20:2, C20:3, C22:3 and C22:4 FAs (Figs. 1*I* and S1). The substantial reduction of FA levels attributed to STAT3 inhibition likely resulted from downregulation of FA synthesis and subsequent desaturation and elongation, impacting the critical genes involved in this process, including FASN, SCD1, fatty acid desaturase 1/2 (FADS1/2), and fatty acid elongase 2/5/6 (ELOVL2/5/6) (Fig. 1*J*) (8, 38, 39). These enzyme alterations may account for the significant changes in both FFA and the phospholipid profile, which were tested in subsequent studies.

Inhibition of STAT3 downregulates a SCAP-SREBP-1-FASN-SCD1 axis in various cancer cells

After dissociation from the ER-resident protein insulin-induced gene (Insig), SCAP promotes SREBP-1 trafficking and nuclear translocation to activate the expression of genes involved in FA synthesis, including *FASN, SCD1, FADS*, and various members of the *ELOVL* gene family (Fig. 2*A*) (6, 7, 18, 39). We investigated whether SREBP-1 regulates the expression of these genes in GBM U251 cells. Pharmacological inhibition of SREBP-1 using its inhibitor fatostatin (Fato, 24 h) and shRNA knockdown of SREBP-1 led to a significant reduction in the expression of *SREBP-1a*, *SREBP-1c*, *FASN*, *SCD1*, *FADS1, FADS2*, *ELOVL2, ELOVL5* and *ELOVL6* (Fig. 2, *B* and *C*). We next investigated whether STAT3 inhibition possibly affected the expression of *SCAP* and *SREBF1* (encoding SREBP-1) expression, thereby leading to reduced expression of downstream genes involved in FA synthesis. Real-time PCR analysis revealed that pharmacological inhibition of STAT3 with Napa significantly decreased the expression of *SCAP, SREBP-1a*, *SREBP-1c, FASN*, *SCD1*, *FADS1/2*, as well as the *ELOVL2/5/6* genes in U251 cells (Fig. 2*D*).

We also investigated whether STAT3 inhibition had an impact on the protein levels of these factors. By Western blotting, we found a significant reduction in SCAP levels, as well as the SREBP-1 precursor (P) and N-terminal (N) active forms in multiple cancer types, including GBM (U251, GBM30, U373, T98 and U87), lung cancer (A549 and H1299), and liver cancer (HepG2), when compared to untreated cells (Figs. 2*E* and S2*A*). The protein disulfide isoform (PDI), an ER membrane protein used as the loading control for SCAP, remained unchanged (Fig. 2*E*). Furthermore, through Western blotting analysis, we demonstrated that downstream targets of the SCAP-SREBP-1 pathway, namely FASN and SCD1, responsible for FA synthesis and desaturation, exhibited significantly reduced levels in Napa-treated cells in comparison to untreated cells (Figs. 2*E* and S2*A*). In addition, we tested three other STAT3 inhibitors, TTI-101 (currently in Phase II clinical trials), HO-3867, and LLL12 using GBM30 cells (40–42). Notably, all three inhibitors demonstrated similar effects as Napa in reducing the SCAP-SREBP-1 pathway (Fig. S2, *B* and *C*). To strengthen the causal link between STAT3 and the SCAP-SREBP-1-FASN-SCD1 pathway, we employed genetic inhibition of STAT3 using two distinct lentivirus-mediated shRNAs. This genetic inhibition (Fig. 2*F*) mirrored the results of pharmacological inhibition (Fig. 2*E*)

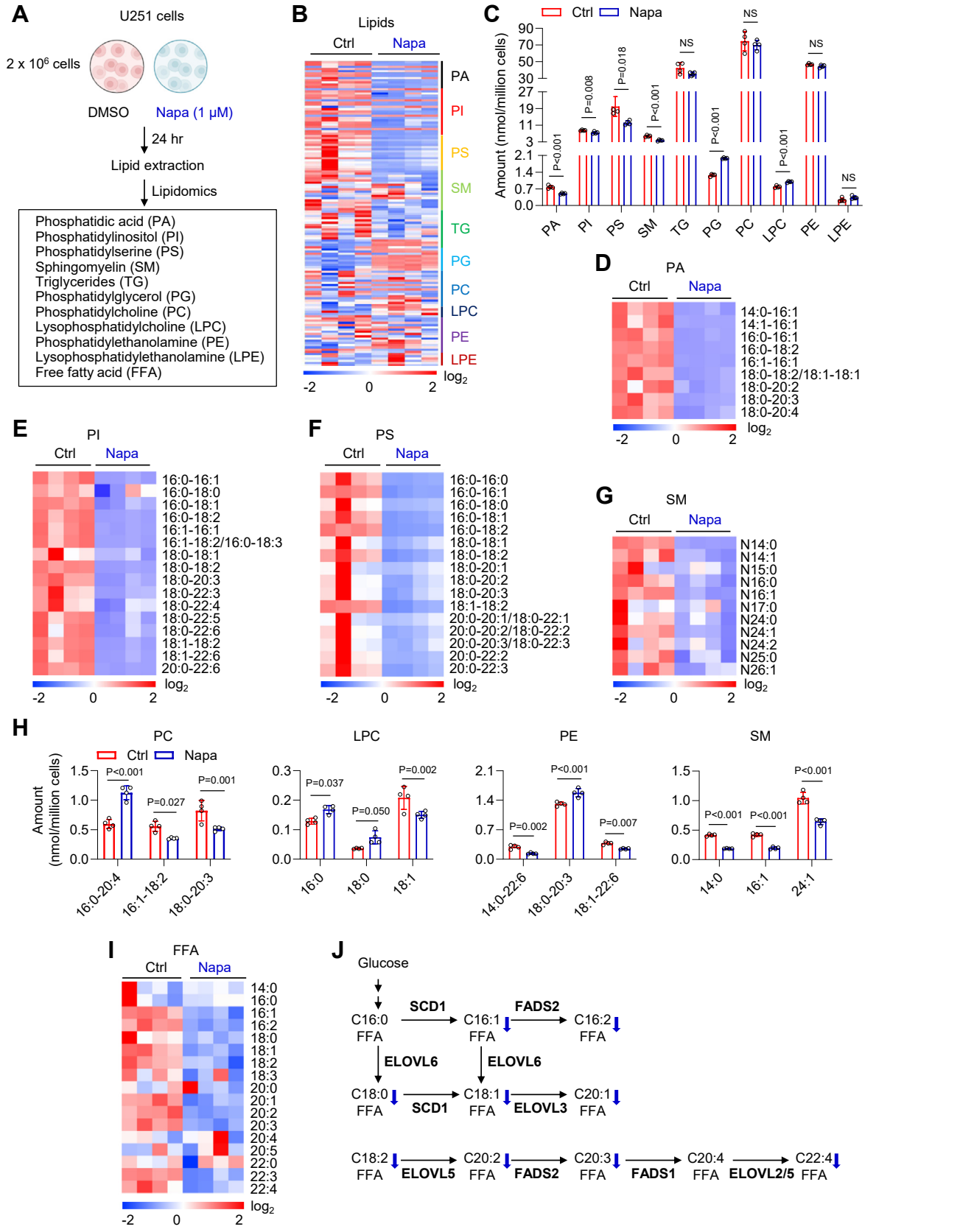

Figure 1. Inhibition of STAT3 significantly reduces free FA levels and disrupts phospholipid homeostasis in GBM cells. *A*, a schematic diagram illustrating the lipidomic analysis of GBM U251 cells treated with or without napabucasin (Napa, 1 μM) in serum-free DMEM medium for 24 h. *B*, heatmap of different lipids in U251 cells collected from *panel A* ($n = 4$). *C*, total levels of each type of lipids in U251 cells with or without Napa treatment. The data is shown as mean ± S.D. ($n = 4$). *D–G*, heatmap of individual species of PA, PI, PS, and SM in U251 cells with or without Napa treatment ($n = 4$). *H*, levels of representative individual lipid species of PC, LPC, PE and SM in U251 cells with or without Napa treatment. The data is shown as mean ± S.D. ($n = 4$). *I*,

and led to a substantial decrease in the protein levels of SCAP, SREBP-1 precursor, and active forms (P and N), as well as FASN and SCD1 in GBM, lung, and liver cancer cells.

We proceeded to investigate whether the changes in lipid profiles induced by STAT3 inhibition using Napa resulted in cell death. Notably, Napa treatment led to highly significant cell death in both U251 and H1299 cells when compared to control treatment (Fig. 2, *G* and *H*). Next, we examined whether the supplementation of palmitoleic acid (POA, C16:1) and/or oleic acid (OA, C18:1), the two most abundant monounsaturated FAs in many cells, could rescue the cell death induced by Napa treatment. Interestingly, the supplementation of a mixture of bovine serum albumin (BSA)-conjugated POA and OA at a ratio of 1:4 according to their levels in tumor cells as demonstrated by lipidomics analysis (Fig. S1), effectively rescued the cell death induced by Napa treatment in both cell lines, whereas supplementation with either POA or OA alone failed to do so (Fig. 2, *G* and *H*). The combined rescue effects were dose-dependent from 5 to 10 μM POA and 20 to 40 μM OA, with a maximal effect at the combination of 10 μM POA and 40 μM OA (Fig. S2*D*). In contrast, supplementing saturated FAs, palmitic acid (C16:0), stearic acid (SA, C18:0), polyunsaturated FAs linoleic acid (LA, C18:2), and a ternary mixture of them into cancer cells did not have rescue effects on Napa-induced cell death (Fig. S2*E*). As with the rescue of Napa treatment, supplementing fatty acids (POA and OA) also significantly rescued cell viability in GBM and lung cancer cells with STAT3 shRNA knockdown (Fig. 2, *I* and *J*). These results underscore the essential role of both monounsaturated FAs in supporting cancer cell growth.

In summary, our data demonstrate that STAT3 inhibition downregulates the SCAP-SREBP-1-FASN-SCD1 signaling pathway, thereby disrupting the regulation of *de novo* FA synthesis and desaturation processes in cancer cells, ultimately leading to their death.

STAT3 binds to the promoters of SCAP *and* SREBF1 *to activate their expression*

To elucidate the underlying mechanism by which STAT3 regulates SCAP and SREBP-1 expression, we utilized the JASPAR database for analysis of potential transcription factor binding sites (43, 44) within the promoters of *SCAP* and *SREBF1*. The *SREBF1* gene encodes both SREBP-1a and -1c proteins through the utilization of alternative promoters within the same gene (24, 45–47). Our analysis revealed the presence of multiple potential STAT3 binding motifs in the promoters of *SCAP* and *SREBP1* (Fig. 3, *A–C*). To validate these putative binding sites, we designed corresponding primers flanking them (Fig. 3, *A–C*). Subsequently, we conducted chromatin immunoprecipitation using an anti-STAT3 antibody in four cancer cell lines U251 and U373 (GBM), A549, and H1299 (lung cancer). The precipitated DNA was then analyzed through real-time PCR using the specifically designed primers (Fig. 3, *A–C*, top scheme). Our results confirmed that STAT3 indeed binds to the predicted sites within the *SCAP* and *SREBF1* promoters (Fig. 3, *A–C*).

To further confirm the binding and activation of gene expression from the *SCAP* promoter and the two alternative promoters of *SREBF1* by STAT3, we cloned these promoters into pGL3-luciferase (luc) promoter-based reporter plasmid, denoted as pGL3-*SCAP*-luc, pGL3-*SREBP-1a*-luc, and pGL3-*SREBP-1c*-luc. Each of these plasmids was individually co-transfected into GBM cell lines (U251 and U373) and the lung cancer cell lines (A549 and H1299) along with either pcDNA3.1 (serving as a control) or pcDNA-STAT3 for 48 h. Bioluminescence analyses revealed that STAT3 expression led to a significant increase in the activity of the *SCAP*, *SREBP-1a,* and *-1c* promoter in each cell line. This was evidenced by higher levels of luciferase activity when compared to the control pcDNA3.1 plasmid transfection (Fig. 3*D*).

In summary, these findings confirm that STAT3 functions as a direct transcription factor, coordinating the expression of SCAP and SREBP-1, resulting in a rapid increase in FA levels and ultimately promoting tumor growth.

Inhibition of STAT3 downregulates SCAP and SREBP-1 in a GBM xenograft model

We proceeded to investigate whether the pharmacological inhibition of STAT3 could have the same downregulatory effects on SCAP and SREBP-1 expression, as well as their downstream FA synthesis enzymes in an *in vivo* setting. To do this, we implanted 2×10^6 GBM30 cells into the flanks of mice to establish a xenograft model. After 1 week, the tumor volumes reached approximately 80 mm^3, at which point we initiated treatment by administering Napa (40 mg/kg/2 days *via i.p.*) for 2 weeks. Our results demonstrated that Napa treatment significantly suppressed tumor growth, as evidenced by reduced tumor volume and weight (Fig. 4, *A–C*). Immunohistochemistry (IHC) analysis revealed that Napa treatment led to a considerable reduction in STAT3 phosphorylation at Tyr705, as well as decreased expression of SCAP, SREBP-1, FASN, and SCD1 (Fig. 4*D*). Furthermore, there was a significant decrease in Ki67 staining, a marker of tumor proliferation, in the tumor tissues compared to the control group (Fig. 4*D*). We also examined clinical samples from patients with GBM. IHC staining of these samples indicated a strong correlation between high levels of STAT3 phosphorylation at Tyr705 and elevated levels of SCAP, SREBP-1, FASN, and SCD1 in tumor tissues. In contrast, their levels were low in the adjacent normal tissues (Fig. 4*E*).

heatmap of free fatty acids (FFAs) in U251 cells with or without Napa treatment ($n = 4$). *J*, schematic diagram illustrating the pathways of *de novo* FFA synthesis, elongation and desaturation catalyzed by the indicated enzymes and summary of the changes of specific FFAs in U251 cells after Napa treatment as *panel A*. Statistical significance was analyzed by an unpaired Student's *t* test (*C*) or two-way ANOVA with Šídák's multiple comparisons test (*H*). NS, not significant. Please also see Fig. S1. ELOVL2/3/5/6, fatty acid elongase 2/3/5/6; FADS1/2, fatty acid desaturase 1/2; LPC, lysophosphatidylcholine; LPE, lysophosphatidylethanolamine; PA, phosphatidic acid; PC, phosphatidylcholine; PE, phosphatidylethanolamine; PG phosphatidylglycerol; PI, phosphatidylinositol; PS, phosphatidylserine; SCD1, stearoyl-CoA desaturase 1; SM, sphingomyelin; TG, triglycerides.

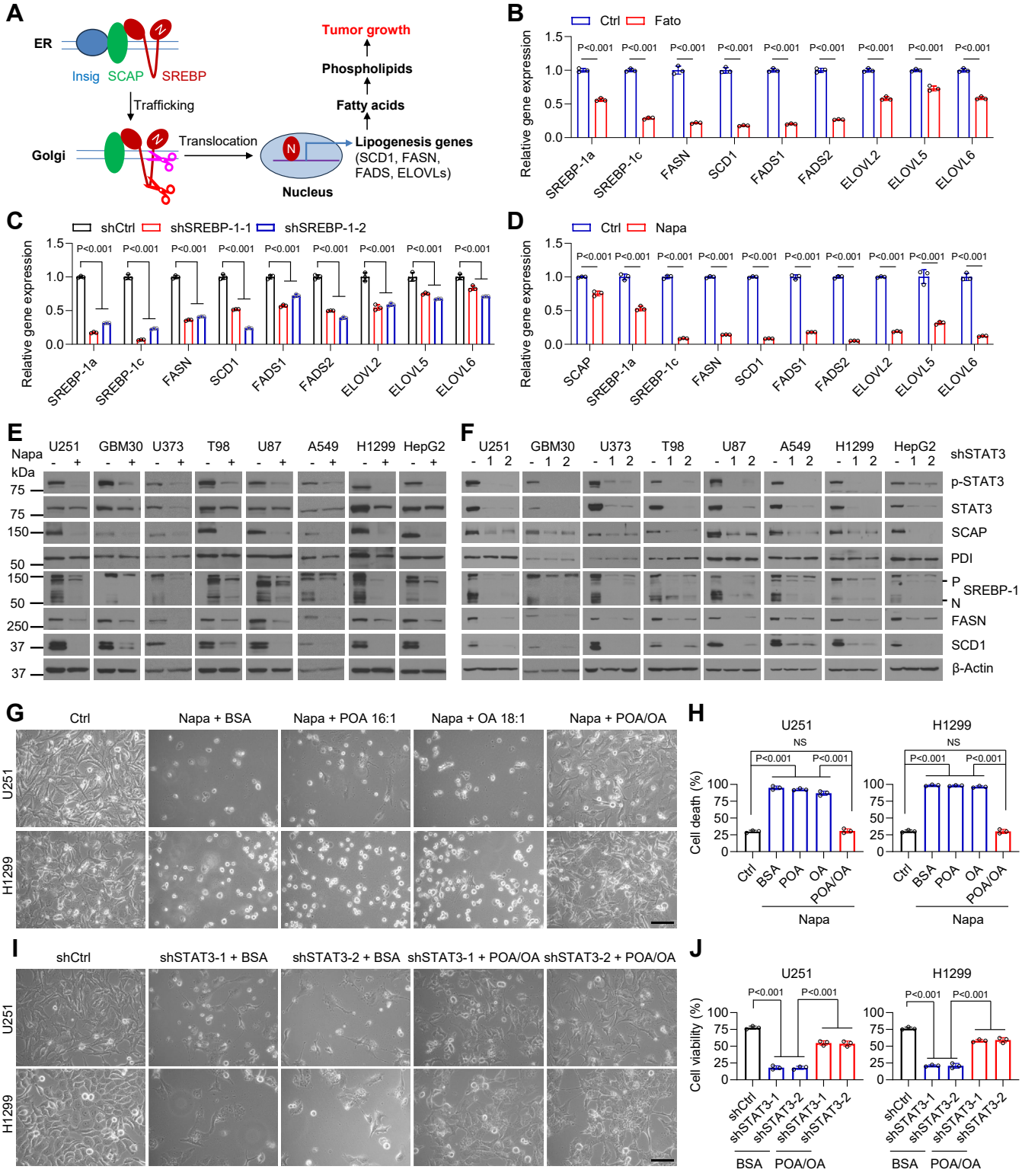

Figure 2. Inhibiting STAT3 suppresses SCAP and SREBP-1 expression and downregulates FA synthesis enzyme levels. *A*, a schematic diagram illustrating the pathway by which SCAP transports SREBP-1 from the endoplasmic reticulum (ER) to the Golgi after dissociation from the ER-resident protein Insig. In the Golgi, SREBP-1 is sequentially cleaved by two proteinases, which releases the N-terminal active SREBP-1 form that enters nucleus to activate the expression of FA synthesis-related genes to promote phospholipid formation and tumor growth. *B* and *C*, real-time PCR analysis of gene expression in U251 cells with or without fatostatin (10 μM) in serum-free medium for 24 h (*B*) or infection with two different lentivirus-mediated shRNA against SREBP-1 as compared with scramble shRNA (shCtrl) for 72 h (*C*). The data is shown as mean ± S.D. ($n = 3$). *D*, real-time PCR analysis of gene expression in U251 cells with or without Napa (1 μM) treatment in serum-free medium for 24 h. The data is shown as mean ± S.D. ($n = 3$). *E* and *F*, Western blot analysis of membrane (for SCAP and PDI) and whole lysates (for STAT3, p-STAT3, SREBP-1, FASN and SCD1) in U251, U373, T98, U87, A549, H1299, HepG2 cells (1 μM) in 1% FBS, or in primary GBM30 cells (5 μM) in 0.1 × B-27 medium with or without Napa treatment (*E*) for 24 h, or lentivirus-mediated shRNA knockdown of STAT3 for 72 h (*F*). Protein disulfide-isomerase (PDI), an ER-resident protein as SCAP internal control. *G* and *H*, representative micrographs of U251 and H1299 cells supplemented with BSA-conjugated palmitoleic acid (POA, 10 μM) and oleic acid (OA, 40 μM) alone or combination for 24 h, followed by treatment with or

Discussion

Aberrant activation of STAT3 signaling and exaggerated FA synthesis are two prominent characteristics of various human cancers (31, 48–50). However, whether these two pathways have an intrinsic causal connection has been unclear. Our current study revealed that STAT3 binds to, and induces the promotion of, both *SCAP* and *SREBF1* expression in various cancer cells. This upregulation promotes FA synthesis and phospholipid generation to support tumor growth. Notably, we characterized the lipid landscape in tumor cells after STAT3 inhibition using mass spectrometry-based lipidomics analysis and found markedly decreased levels of unsaturated FAs and phospholipids containing unsaturated FA chains. To the best of our knowledge, this is the first report to perform lipidomics in STAT3-related studies. Moreover, mono-unsaturated fatty acid, like oleic acid (OA, C18:1), is critical for cancer cell growth (9–11), while the role of palmitoleic acid (POA, C16:1) has not been sufficiently emphasized before. The production of POA is also regulated by SCD1, which converts palmitate acid (PA, C16:0) to POA (C16:1) (6–8). POA can further be converted to oleic acid (OA, C18:1) by ELOVL6 (7). As inhibition of STAT3 by Napa significantly reduces both POA and OA levels (Figs. 1*I* and S1), rescuing cell death induced by Napa requires adding both. In summary, our findings unveil the underlying molecular connection between oncogenic STAT3 signaling and *de novo* FA synthesis, providing insights into understanding how tumor cells coordinate the hyperactive oncogenic signaling and acquisition of sufficient lipid building blocks to promote rapid tumor growth.

The rate-limiting step controlling SREBP-1 activation and its downstream FA synthesis enzyme expression is SCAP dissociation from the ER-resident protein Insig, which then facilitates SREBP-1 trafficking and subsequent nuclear translocation (1, 2, 17, 18, 24). In addition to the regulation by nutrients, *that is,* cholesterol, glucose, glutamine, and ammonia (1–3, 17, 18, 21), a previous study from Brown & Goldstein's group showed that the stoichiometry between SCAP and Insig protein levels in Chinese hamster ovarian (CHO) cells can also modulate SREBP trafficking (26). When SCAP protein levels significantly exceed Insig, the unbound SCAP (*i.e.*, the portion not binding to Insig) can transport SREBPs from the ER to the Golgi for cleavage and activation (26). This result has been confirmed by our group. We showed that overexpression of SCAP strongly activates SREBP-1 and FASN-SCD1 expression and promotes rapid tumor growth in GBM and lung cancer xenograft models (3, 21). Our current study unveiled that STAT3 plays a dual function in the regulation of the SCAP-SREBP-1 pathway. It simultaneously upregulates the gene and protein expression of both SCAP and SREBP-1. The abundant SCAP can overcome the restriction of Insig in the ER, thereby allowing high level of SREBP-1 protein trafficking and nuclear translocation, leading to high levels of FA production to promote tumor growth. Interestingly, a recent study reported that STAT3 can also transcriptionally regulate SREBP-2 expression to increase cholesterol synthesis in triple-negative breast cancer cells (51), which together with our current study demonstrates STAT3 plays an important role in regulating lipid metabolism in various cancers.

Pharmacologically targeting FA synthesis by inhibiting the key enzymes, *i.e.*, acetyl-CoA carboxylation (ACC), FASN, and SCD1, has been extensively tested in preclinical xenograft models (52–57). Among these enzyme inhibitors, TVB-2640 for FASN, has been tested in Phase II/III clinical trials to treat high-grade astrocytoma, GBM, lung, and breast cancers (58, 59); while PF-05221304 for ACC is in Phase I/II clinical trials to treat non-alcoholic fatty liver disease (60–62) and MK-8245 for SCD1 is in Phase I clinical trials to treat type 2 diabetes. Nevertheless, we know now that all monotherapies, particularly for treating solid tumors, almost unavoidably lead to the development of tumor resistance, usually in a rapid fashion. We envision that if the protein levels of FA synthesis-related enzymes were reduced, their inhibitors would work more potently. Recently, several small molecular inhibitors to block SCAP-SREBP-1 trafficking to reduce FA synthesis have been reported, such as fatostatin (63, 64), while none of them have been translated to the clinic to test in patients. As inhibition of STAT3 by the clinically tested inhibitor Napa can efficiently reduce FASN and SCD1 protein levels by inhibition of SCAP-SREBP-1 as shown by our current study, combining a STAT3 inhibitor with FA synthesis enzyme inhibitors may produce a strong synergistic effect to suppress tumor growth by dramatically reducing FA availability. In addition, recent studies from other groups reported that STAT3 transcriptionally regulates the expression of CD36, a fatty acid transporter, facilitating FA uptake in leukemia and breast cancer (65–68). Thus, the combination of a STAT3 inhibitor with FA metabolism inhibitors may be very effective in treating various cancers. We will test this combination in future studies.

Experimental procedures

Human glioblastoma samples

Human glioblastoma samples used in this study are de-identified. Biopsies from individuals were obtained from the Department of Pathology at the Ohio State University Medical Center and the UCLA Medical Center after surgery and were fixed in 4% paraformaldehyde for 24 h, then embedded in paraffin. Analysis of tissues from individuals was approved by the Ohio State University Institutional Human Care and Use Committee.

without Napa (U251, 0.5 μM; H1299, 0.4 μM) for 72 h (*G*). Live and dead cells were quantified (*H*) by hemocytometer after trypan blue staining. Cell death percentage was determined by the ratio of dead cells *versus* total cell number (live + dead). The data is shown as mean ± S.D. (n = 3). Scale bar, 100 μm. *I* and *J*, representative micrographs of U251 and H1299 cells with lentivirus-mediated shRNA knockdown of STAT3 in serum-free medium supplemented with BSA-conjugated palmitoleic acid (POA, 5 μM) and oleic acid (OA, 20 μM) combination for 72 h (*I*). Live and dead cells were quantified (*J*) by hemocytometer after trypan blue staining. Cell viability was determined by the ratio of live cells *versus* total cell number (live + dead). The data is shown as mean ± S.D. (n = 3). Scale bar, 100 μm. Statistical significance was analyzed by one-way ANOVA with Tukey's multiple comparisons test (*J* and *H*) or two-way ANOVA with Šídák's multiple comparisons test (*B–D*). NS, not significant. Please also see Fig. S2. N, N-terminus of SREBP-1; P, precursor of SREBP-1.

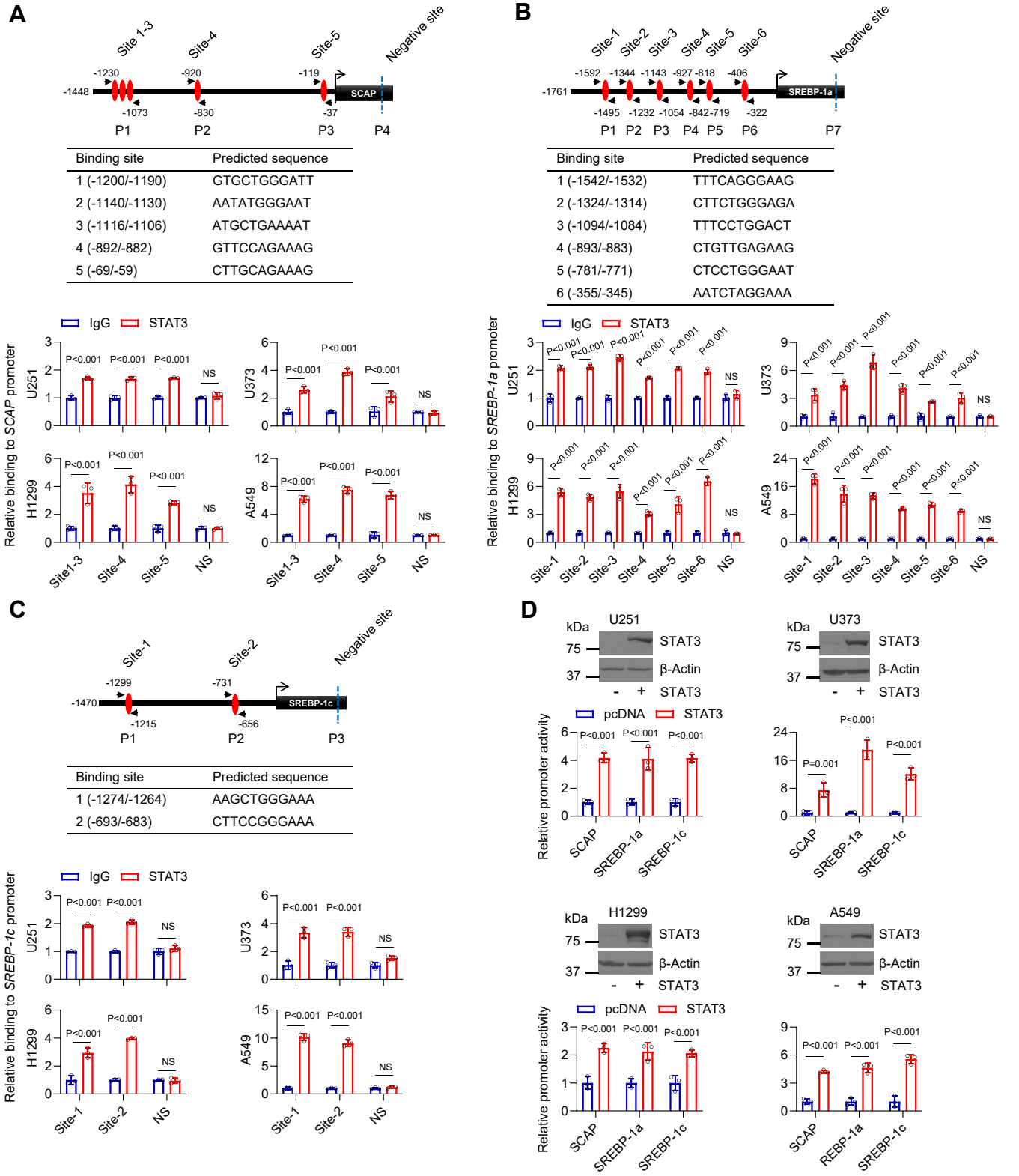

Figure 3. STAT3 binds *SCAP* and *SREBF1* promoters to activate their expression. *A–C, upper panels* (scheme) show the putative STAT3 binding sites on promoters and negative binding site (NS) on exons of *SCAP* (A), *SREBP-1a* (*B*), and *SREBP-1c* (*C*) gene. Inserted tables under schemes show the detailed predicted STAT3-binding motifs in each gene promoter. *Bottom panels* show the results of ChIP-PCR analysis of STAT3 binding to the predicted sites in each promoter and NS motifs in exon in U251, U373, A549 and H1299 cells. The data were shown as mean ± S.D. (n = 3). *D*, promoter reporter luciferase (luc) activity (*bottom panels*) for respective gene promoters containing STAT3 binding motifs shown in the diagrams (*A–C*) cloned in the pGL3-luc basic vector that were transfected into U251, U373, A549 or H1299 cells together with pRL-TK-Renilla, pcDNA3.1, pcDNA3.1-STAT3 for 48 h. Western blot analysis (*upper panels*) of STAT3 with pcDNA3.1, pcDNA3.1-STAT3 transfection into the corresponding cells for 48 h. The data is shown as mean ± S.D. (n = 3). Statistical significance was analyzed by two-way ANOVA with Šídák's multiple comparisons test (*A–D*).

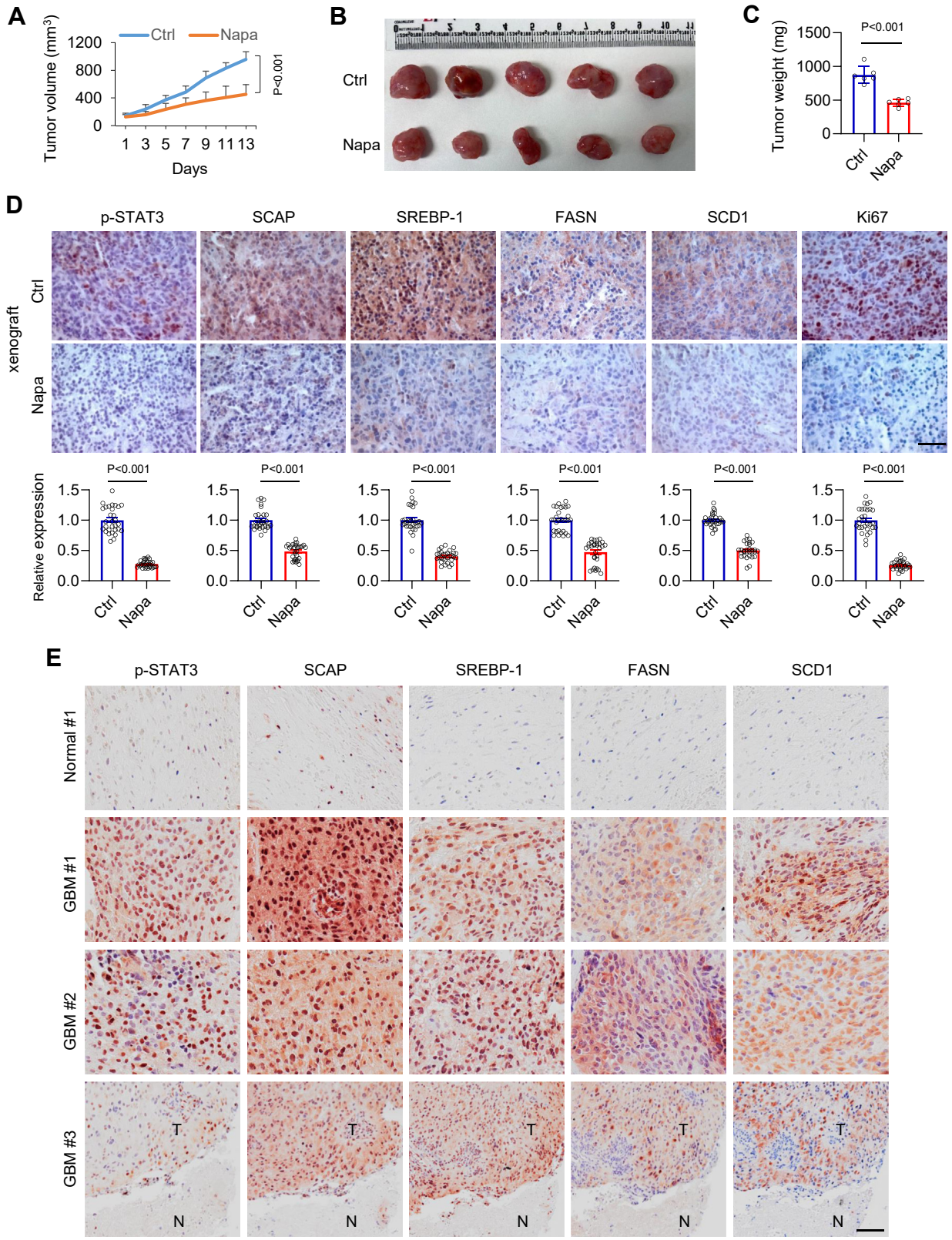

Figure 4. Pharmacological inhibition of STAT3 downregulates SCAP and SREBP-1 in a GBM xenograft model to shrink tumor volume. *A–C*, tumor growth curve of GBM30-derived subcutaneous xenografts (mean ± S.D., $n = 6$) treated with Napa (40 mg/kg/2 days, *i.p.*) for 14 days (*A*). Tumors were imaged after 14 days of treatment (*B*) and weighed (*C*). *D*, representative images of immunohistochemistry (IHC) staining (*top*) and their quantitation (*bottom*) of indicated proteins in tumor tissues from *panel B*. Five separate areas from each tumor were quantified by ImageJ (mean ± SEM). Scale bar, 50 μm. *E*, representative images of IHC staining of indicated proteins in GBM tumor (T) *versus* adjacent normal (N) brain tissues from human patients. Scale bar, 50 μm. Statistical significance was analyzed by two-way ANOVA with Šídák's multiple comparisons test (*A*) or Student's *t* test (*C* and *D*).

Xenograft mouse model

A xenograft model was generated using female athymic nude mice (NCr-nu/nu, 6–8 weeks) obtained from the OSU Target Validation Shared Resource. GBM30 cells (2×10^6) were suspended in 100 μl PBS with 50% Matrigel and implanted in the mouse flank. The mice were randomly divided into 2 groups after implantation for drug treatment. Napabucasin (40 mg/kg/2 days) formulated with 10% DMSO/10% Tween 80 in PBS and vehicle was administrated to mice by *i.p.* when tumor size reached approximately 80 mm^3. Mice were housed at a maximum of 5 per cage in a conventional barrier facility with free access to water and food on a 12 h light/12 h dark cycle at 22 °C and a relative humidity of 25%. Mouse health status was monitored by following the approved protocols. All animal procedures were approved by the Subcommittee on Research Animal Care at the Ohio State University Medical Center.

Materials

Napabucasin (HY-13919), TTI-101 (HY-112288), HO-3867 (HY-100453), stearic acid (C18:0, HY-B2219), and linoleic acid (C18:2, HY-N0729) were purchased from MedChemExpress. LLL12 (#1792) was from BioVision. Fatostatin (#5533803) was from ChemBridge Corp Antibodies for STAT3 (#9139), phospho-STAT3 (Tyr705, #9145), FASN (#3180), SCD1 (#2438), anti-mouse IgG (HRP-linked antibody, #7076), and anti-rabbit IgG (HRP-linked antibody, #7074) were purchased from Cell Signaling. SREBP-1 antibody (#557036) was from BD Pharmingen. SCAP antibody (#A303-554A) was from Bethyl Laboratories. PDI antibody (sc-30932) and palmitoleic acid (C16:1, sc-205424A) were from Santa Cruz Biotechnology. Beta-actin (#A1978) antibody, normal mouse IgG (#NI03), oleic acid (C18:1, #O1383), palmitic acid (C18:1, #P9417), bovine serum albumin (#A7030), human EGF (#E9644), Heparin (#H3393) and trypan blue solution (#T8154) were from Sigma-Aldrich. Recombinant Human FGF (#4114-TC-01M) was from R&D Systems. B-27 Supplement (#12587010) was from Fisher. Antibodies for STAT3 and phospho-STAT3 were validated by shRNA knockdown of STAT3, and other antibodies were validated by our previous publications (3, 9, 21, 69).

Cell culture

Human glioblastoma (GBM) cell lines U251, U373, T98, and liver cancer cell line HepG2 from American Type Culture Collection (ATCC) were cultured in Dulbecco's modified Eagle's medium (DMEM) supplemented with 5% fetal bovine serum (FBS) at 37 °C in 5% CO_2. Human lung cancer cell lines A549 and H1299 from ATCC were cultured in RPMI 1640 supplemented with 5% FBS. These cell lines were validated by short tandem repeat profiling. Primary GBM patient-derived cells GBM30 were cultured in DMEM/F12 supplemented with B-27 (1×), heparin (2 μg/ml), EGF (20 ng/ml) and fibroblast growth factor (FGF, 20 ng/ml).

Lipidomics analysis

2×10^6 U251 cells were plated in 15 cm dishes and incubated overnight, then washed once with PBS and treated with DMSO or 1 μM napabucasin in serum-free medium for 24 h. Cultured cells were collected using trypsin, then centrifuged at 500*g* for 5 min, and washed with cold PBS for three times.

Cell pellets were homogenized on ice with 0.5 ml of 0.1× PBS at 6500 rpm, 0 °C in 2 ml Precellys Lysing tube (Bertin) using Cryolys Evolution homogenizer (Precellys Evolution). The protein concentration of cell homogenates was quantified using the Pierce BCA protein assay kit (#23225, Thermo Scientific). Bovine serum albumin was used as standard. An adequate amount of each homogenate (equivalent to 0.64 mg protein) was transferred into a disposable glass culture test tube. The same lipid internal standard mixture for quantitation of lipids was added prior to lipid extraction. Lipid extraction was performed using a modified Bligh and Dyer procedure, as described previously (70). Lipid extracts were flushed with nitrogen, capped, and stored at −20 °C until lipid analysis.

Shotgun lipidomics was performed as described previously (71). Lipid extract was further diluted to a final concentration of ∼500 fmol total lipids per μL. Mass spectrometric analysis was performed on a triple quadrupole mass spectrometer (TSQ Altis, Thermo Fisher Scientific) and a Q Exactive mass spectrometer (Thermo Scientific, San Jose, CA), both of which were equipped with an automated nanospray device (TriVersa NanoMate, Advion Bioscience Ltd, Ithaca, NY) as described (72). Identification and quantification of lipid species were performed using an automated software program (73, 74). Data processing (*e.g.*, ion peak selection, baseline correction, data transfer, peak intensity comparison, and quantitation) was performed as described (74). Data were normalized per million cells. Reproducibility by analyzing a prepared sample by multidimensional mass spectrometry-based shotgun lipidomics (MDMS-SL) is approximately 95%, and precision is approximately 90%, largely due to variations in determining protein content for normalizing lipid levels. The content of lipids was analyzed and quantified by the GraphPad Prism 10 software and heatmap. Heatmaps were generated using MultiExperiment Viewer (MeV) software, and Z score of each lipid for each replicate was calculated by subtracting its mean and then dividing by its standard deviation across two groups.

Quantitative real-time PCR

Total RNA was isolated from cells with TRIzol (15596018, Fisher) according to the manufacturer's protocol, and cDNA was synthesized with iScript cDNA Synthesis Kit (1708891, Bio-Rad). Quantitative real-time PCR was performed with PowerUp SYBR Green Master Mix (A25778, Fisher) using the Applied Biosystems QuantStudio 6 Pro RealTime PCR System (Thermo Fisher Scientific). The expression was normalized to the 36B4 housekeeping gene and calculated with the comparative method ($2^{-\Delta\Delta Ct}$). The primers are listed in Table 1.

Table 1
Primers for quantitative real-time PCR

Gene	Primer	Sequence
SCAP	Forward	5′-TCCTCATCGGCTACTTCACC-3′
	Reverse	5′-TCGCTTGTTCAGGTCTGCTA-3′
SREBP-1a	Forward	5′-TCAGCGAGGCGGCTTTGGAGCAG-3′
	Reverse	5′-CATGTCTTCGATGTCGGTCAG-3′
SREBP-1c	Forward	5′-GGAGCCATGGATTGCACATT-3′
	Reverse	5′-TCGTTTGTACCCGTTGATGA-3′
FASN	Forward	5′-GTTCACGGACATGGAGCAC-3′
	Reverse	5′-GTGGCTCTTGATGATCAGGTC-3′
SCD1	Forward	5′-TGCGATATGCTGTGGTGCT-3′
	Reverse	5′-GATGT CCAGCGGTACTCA-3′
FADS1	Forward	5′-CTGTCGGTCTTCAGCACCTCAA-3′
	Reverse	5′-CTGGGTCTTTGCGGAAGCAGTT-3′
FADS2	Forward	5′-TGCAACGTGGAGCAGTCCTTCT-3′
	Reverse	5′-GGCACATAGAGACTTCACCAGC-3′
ELOVL2	Forward	5′-TCCACTTGGGAAGGAGGCTACA-3′
	Reverse	5′-CCAGGAACTCTACTGATTTGGAG-3′
ELOVL5	Forward	5′-ACGTCTACCACCATGCCTCGAT-3′
	Reverse	5′-TGGAAGGGACTGACGACAAACC-3′
ELOVL6	Forward	5′-CCATCCAATGGATGCAGGAAAAC-3′
	Reverse	5′-CCAGAGCACTAATGGCTTCCTC-3′
36B4	Forward	5′-AATGGCAGCATCTACAACCC-3′
	Reverse	5′-TCGTTTGTACCCGTTGATGA-3′

Lentiviral transduction

Mission pLKO.1-puro lentivirus vector containing shRNA for STAT3 (1, TRCN0000020843; 2, TRCN0000329887), SREBP-1 (1, TRCN0000414192; 2, TRCN0000421299) and the non-mammalian shRNA control (SHC002) were from Sigma-Aldrich. The shRNA vector and packing plasmids psPAX2 and the envelope plasmid pMD2.G were transfected into 293FT cells using the polyethyleneimine. Supernatants were harvested at 48 h, 72 h and concentrated using the Lenti-X Concentrator (631232, Takara). The virus titer was quantified by real-time PCR by using qPCR Lentivirus Titration Kit. The lentiviral transduction was performed according to Sigma's MISSION protocol with polybrene (8 μg/ml). The cancer cells were infected with the same multiplicity of infection of shRNA.

Western blotting

Cells were lysed by RIPA buffer containing a protease inhibitor cocktail and phosphatase inhibitor. The proteins were separated by using 12% SDS-PAGE and transferred onto an ECL nitrocellulose membrane. After blocking for 1 h in 5% nonfat milk diluted by Tris-buffered saline containing 0.1% Tween 20, the membranes were incubated with various primary antibodies, followed by secondary antibodies conjugated to horseradish peroxidase. The immunoreactivity was revealed by use of an ECL kit.

Preparation of cell membrane fractions

Cell membranes were isolated as previously described (75, 76). Cells were washed once with PBS and harvested by scraping. Cells were resuspended in a buffer containing 10 mM HEPES-KOH (pH 7.6), 10 mM KCl, 1.5 mM $MgCl_2$, 1 mM sodium EDTA, 1 mM sodium EGTA, 250 mM sucrose, and a mixture of protease inhibitors, 5 μg/ml pepstatin A, 10 μg/ml leupeptin, 0.5 mM PMSF, 1 mM DTT, and 25 μg/ml ALLN for 30 min on ice. Extracts were passed through a 22G × 1-1/2 inch needle 30 times and centrifuged at 890*g* at 4 °C for 5 min to remove nuclei. The supernatants were centrifuged at 20,000*g* for 20 min at 4 °C. For subsequent Western blot analysis of SCAP protein, the pellet was dissolved in 0.1 ml of SDS lysis buffer (10 mM Tris-HCl pH 6.8, 100 mM NaCl, 1% (v/v) SDS, 1 mM sodium EDTA, and 1 mM sodium EGTA) and designated as 'membrane fraction'. The membrane fraction was incubated at 37 °C for 30 min, and protein concentration was determined. 1 μl of bromophenol blue solution (100 ×) was added before the samples were subjected to SDS-PAGE.

Fatty acids preparation

FAs conjugated to the BSA solution were prepared as described previously (77). FAs were dissolved in 0.1 M of NaOH to yield a 50 mM concentration and heated while stirring at 70 °C for unsaturated FAs or 90 °C for saturated FAs until dissolved (a few seconds). A 0.2 ml aliquot of the resulting fatty acid solution was added while stirring into 1.2 ml of a 10% BSA solution at 37 °C. After 15 min of slow stirring to allow clarification of the solution, 0.6 ml of water was added to bring the final concentration to 5 mM of fatty acid. The solutions were filtered through a 0.22 μm filter and stored at −80 °C. The molar ratio of BSA and FAs in BSA-conjugated FAs was approximately 1:5.5.

Cell proliferation assay

In lipid rescue experiments, U251, H1299 cells were plated in 6-well plates and incubated overnight, then washed once with PBS and pretreated with 9.1 μM BSA, 10 μM palmitoleic acid, 40 μM oleic acid, 10 μM palmitoleic acid plus 40 μM oleic acid in serum-free medium for 24 h, then treated with napabucasin (U251 cells: 0.5 μM, H1299 cells: 0.4 μM) for 72 h. Cell numbers were counted using a hemocytometer, and dead cells were distinguished by trypan blue solution.

Chromatin immunoprecipitation assay

The ChIP assay was performed using SimpleChIP Plus Enzymatic Chromatin IP Kit (9005S, Cell Signaling) according to the manufacturer's protocol. Briefly, cells in 15 cm dishes were fixed with formaldehyde at a final concentration of 1% and then incubated with glycine, lysed in buffers A and B, digested with micrococcal nuclease, centrifuged to get the pellet nuclei, sonicated in ChIP buffer to harvest the cross-linked chromatin. 3 μg anti-STAT3 or anti-mouse IgG antibodies with protein G magnetic beads were added to each ChIP reaction and incubated overnight. After low salt washing three times and high salt washing one time, each ChIP reaction was eluted using ChIP elution at 65 °C for 0.5 h. The cross-links were reversed using NaCl and proteinase K and incubated at 65 °C for 2 h. Purified DNA was analyzed by quantitative real-time PCR using designed primers (Table 2).

SREBP-1a, SREBP-1c, and SCAP promoter constructs

For all genes, luciferase (luc) reporter constructs were obtained by cloning promoter DNA region into the pGL3-luc vector (Promega). PCR fragments were amplified from genomic DNA using primers where suitable restriction sites were added in the 5′ end (Table 3), then cloned into pGemT vector (Promega) and sequenced.

For *SCAP*, the PCR fragment generated with the specific primers was first cloned into the pGemT vector, then cut KpnI/HindIII and inserted KpnI/HindIII into pGL3-luc to generate pGL3-*SCAP* (−1448/+52)-luc. For *SREBP-1a*, the PCR fragment generated with the specific primers was first cloned into the pGemT vector (Promega), then cut KpnI/BlpI and inserted KpnI/BlpI into pGL3-luc to generate pGL3-*SREBP-1a* (−1761/+194)-luc. pGL3-*SREBP-1c* (−1470/+90)-luc SREBP-1c was obtained as described previously (78).

Promoter-luciferase reporter assay

U251, U373, H1299, A549 cells were seeded in 12-well plates and transiently co-transfected with pcDNA-STAT3 (U251 and U373 cells: 0.5 μg, A549 and H1299 cells: 1 μg), pGL3-*SCAP*-luc, pGL3-*SREBP-1a*-luc, or pGL3-*SREBP-1c*-luc (U251 and U373 cells: SCAP 100 ng, SREBP-1a 50 ng, SREBP-1c, 50 ng; A549 and H1299 cells: SCAP 50 ng, SREBP-1a 20 ng, SREBP-1c, 20 ng) plasmids, and pRL-TK renilla (U251 and U373 cells: 10 ng, A549 and H1299 cells: 5 ng) (Promega) using X-tremeGENE HP DNA Transfection Reagent (6366244001, Roche) for 48 h. The firefly and renilla luciferase activities were measured using Bright-Glo (E2610, Promega) and Renilla-Glo (E2610, Promega) luciferase assay systems. The measurement was performed on a GloMax Discover microplate reader (Promega). For the pcDNA and STAT3 transfection group, average normalized ratio is:

$$\text{pcDNA ratio} = \frac{\text{Target gene promoter–luc/Renilla}}{\text{pGL3–luc/Renilla}};$$

$$\text{STAT3 ratio} = \frac{\text{Target gene promoter–luc/Renilla}}{\text{pGL3–luc/Renilla}}$$

$$\text{Fold Activity} = \frac{\text{STAT3 ratio}}{\text{pcDNA ratio}}$$

Immunohistochemistry

Tissue sections were cut from paraffin blocks of biopsies. Tissue slides were placed in oven at 60 °C for 0.5 h and then deparaffinized in xylene 3 times for 5 min each followed by

Table 2
Primers for chromatin immunoprecipitation assay

Gene	Primer	Sequence
SREBP-1a Site-1	P1-Forward	5′-TCACCCAGCACTTCCTATCC-3′
	P1-Reverse	5′-CCCCACCAACACTCTAGAGG-3′
SREBP-1a Site-2	P2-Forward	5′-GTAATTTTCCACCGCAGCCA-3′
	P2-Reverse	5′-TTTAGAAGGGGTGTGTGGGG-3′
SREBP-1a Site-3	P3-Forward	5′-TTATGAAGGTCTGGGGTCGG-3′
	P3-Reverse	5′-AAGCAGAGAGAAGCACCCTT-3′
SREBP-1a Site-4	P4-Forward	5′-CTAGGCCACAGAACCAGGTT-3′
	P4-Reverse	5′-CTGGATCATCACAAGCTGGG-3′
SREBP-1a Site-5	P5-Forward	5′-CACAGCTACCTCTTCCTTGC-3′
	P5-Reverse	5′-AGTACCCAAGGAAGACTGGC-3′
SREBP-1a Site-6	P6-Forward	5′-GCCTGGGACCCCTATAACTT-3′
	P6-Reverse	5′-CCATCCCAAACTTCATTTCC-3′
SREBP-1a NS	P7-Forward	5′-ACTGAGGTGGAGGACACACT-3′
	P7-Reverse	5′-TCAAAGACTGGGCTGTCAGG-3′
SREBP-1c Site-1	P1-Forward	5′-CCGTCTGTTGTCCTTGAACC-3′
	P1-Reverse	5′-GTCTCTCTCGCAACCTGTCC-3′
SREBP-1c Site-2	P2-Forward	5′-GTGCTGGCAGTCAGGAAAC-3′
	P2-Reverse	5′-GATGAGGCCACTCCTGAAAA-3′
SREBP-1c NS	P3-Forward	5′-CCTTGACAGGTGAAGTCGGC-3′
	P3-Reverse	5′-AAGTGCAATCCATGGCTCCG-3′
SCAP Site1-3	P1-Forward	5′-GGATGGTTTCGATCTCCTGA-3′
	P1-Reverse	5′-AAGTAACAATGGGGACAGTGG-3′
SCAP Site-4	P2-Forward	5′-CTGCCTTGCATTGGTGACTA-3′
	P2-Reverse	5′-ATAAGGCAGGCCCTGTACCT-3′
SCAP Site-5	P3-Forward	5′-CCTTGGACTCCCACAGTGTT-3′
	P3-Reverse	5′-GGCTCTCATCGGTCATCAAG-3′
SCAP NS	P4-Forward	5′-CCACTGCTGAAACTCCCCTT-3′
	P4-Reverse	5′-TAGGCTCTCCTTGTTTGCGG-3′

Table 3
Primers for *SCAP* and *SREBP-1a* promoter constructs

Gene	Primer	Sequence
SCAP	Forward	5′-TGGTACCAAATACCTGTTCCCTGTG-3′
	Reverse	5′-CAAACTTCTCTGGGAGTTCC-3′
SREBP-1a	Forward	5′-GTGGCTCGTCCATGGCGCAGCC-3′
	Reverse	5′-AGAAGCCACAGAGCCCAAGTCC -3′

dipping in graded alcohols (100%, 95%, 80% and 70%) 3 times for 2 min each. Slides were washed with distilled water (dH_2O) 3 times for 5 min each and immersed in 3% hydrogen peroxide for 10 min followed by washing with dH_2O. Slides were transferred into pre-heated 0.01 M Citrate buffer (pH 6.0) in a steamer for 30 min, and then washed with dH_2O and PBS after cooling. Slides were blocked with 3% BSA/PBS at room temperature for 1 h and then incubated with primary antibody overnight at 4 °C, followed by incubating with secondary antibody including Biotinylated Anti-rabbit IgG and Biotinylated Anti-mouse IgG at room temperature for 30 min. After incubation with avidin-biotin complex followed by washing 3 × 5 min with PBS and staining with NovaRed solution, slides were washed with tap water, counterstained with hematoxylin and dipped briefly in graded alcohols (70%, 80%, 95% and 100%) in xylene 2 times for 5 min each. Finally, slides were mounted and imaged.

Statistical analysis

All figures are representative of at least two biological replicates with similar results, unless stated otherwise. Statistical analysis was performed with Excel or GraphPad Prism 10. Lipid amount, gene expression, cell death, binding to promoter, promoter activity, tumor volume, tumor weight, and quantification of IHC intensity were performed using a two-tailed Student's *t* test, as well as by ANOVA, as appropriate. The data are reported as means ± SD. *p* values are indicated in the figure, NS, not significant.

Data availability

All the data reported in this article are available from the correspondence upon request.

Supporting information—This article contains supporting information.

Author contributions—M. P., R. Z., C. W., and Y. F. investigation; F. G., Y. Z., X. M., H. S., Y. K., X. H., Y. F., and A. C. formal analysis; E. L. resources; D. G. and Y. F. conceptualization; D. G. funding acquisition; D. G. supervision; D. G. writing–review & editing; Y. F. writing–original draft

Funding and additional information—This work was supported by the National Institute of Neurological Disorders and Stroke and the National Cancer Institute (USA) grants NS104332, NS112935, CA240726 and CA227874 to D. G. We also appreciate the support from the OSU Comprehensive Cancer Center–Pelotonia Idea grant and Urban & Shelly Meyer Fund for Cancer Research to D. G.

Conflict of interest—The authors declare that they have no known competing financial interests or personal relationships that could have appeared to influence the work reported in this paper.

Abbreviations—The abbreviations used are: ACC, acetyl-CoA carboxylation; BSA, bovine serum albumin; ChIP, Chromatin immunoprecipitation; ELOVL, fatty acid elongase; ER, endoplasmic reticulum; FA, fatty acid; FADS, fatty acid desaturase; FASN, fatty acid synthase; Fato, fatostatin; FBS, fetal bovine serum; FFA, free fatty acid; GBM, glioblastoma; IHC, immunohistochemistry; Insig, insulin-induced gene; LA, linoleic acid; LPC, lysophosphatidylcholine; LPE, lysophosphatidylethanolamine; luc, luciferase; Napa, napabucasin; OA, oleic acid; PC, phosphatidylcholine; PDI, protein disulfide isoform; PE, phosphatidylethanolamine; PG, phosphatidylglycerol; PI, phosphatidylinositol; POA, palmitoleic acid; PS, phosphatidylserine; SA, stearic acid; SCAP, SREBP cleavage-activation protein; SCD1, stearoyl-CoA desaturase 1; SM, sphingomyelin; SREBP-1, sterol regulatory element-binding protein 1; STAT3, signal transducer and activator of transcription 3; TG, triglycerides; Try705, tyrosine 705.

References

1. Cheng, C., Geng, F., Cheng, X., and Guo, D. (2018) Lipid metabolism reprogramming and its potential targets in cancer. *Cancer Commun. (Lond)* **38**, 27
2. Kou, Y., Geng, F., and Guo, D. (2022) Lipid metabolism in glioblastoma: from de novo synthesis to storage. *Biomedicines* **10**, 1943
3. Cheng, C., Ru, P., Geng, F., Liu, J., Yoo, J. Y., Wu, X., *et al.* (2015) Glucose-mediated N-glycosylation of SCAP is essential for SREBP-1 activation and tumor. *Growth Cancer Cell* **28**, 569–581
4. Zaidi, N., Lupien, L., Kuemmerle, N. B., Kinlaw, W. B., Swinnen, J. V., and Smans, K. (2013) Lipogenesis and lipolysis: the pathways exploited by the cancer cells to acquire fatty acids. *Prog. Lipid Res.* **52**, 585–589
5. Koundouros, N., and Poulogiannis, G. (2020) Reprogramming of fatty acid metabolism in cancer. *Br. J. Cancer* **122**, 4–22
6. Horton, J. D., Shah, N. A., Warrington, J. A., Anderson, N. N., Park, S. W., Brown, M. S., *et al.* (2003) Combined analysis of oligonucleotide microarray data from transgenic and knockout mice identifies direct SREBP target genes. *Proc. Natl. Acad. Sci. U. S. A.* **100**, 12027–12032
7. Matsuzaka, T., Shimano, H., Yahagi, N., Kato, T., Atsumi, A., Yamamoto, T., *et al.* (2007) Crucial role of a long-chain fatty acid elongase, Elovl6, in obesity-induced insulin resistance. *Nat. Med.* **13**, 1193–1202
8. Snaebjornsson, M. T., Janaki-Raman, S., and Schulze, A. (2020) Greasing the Wheels of the cancer Machine: the role of lipid metabolism in Cancer. *Cell Metab.* **31**, 62–76
9. Geng, F., Cheng, X., Wu, X., Yoo, J. Y., Cheng, C., Guo, J. Y., *et al.* (2016) Inhibition of SOAT1 suppresses glioblastoma growth via blocking SREBP-1-mediated lipogenesis. *Clin. Cancer Res.* **22**, 5337–5348
10. Hardy, S., St-Onge, G. G., Joly, E., Langelier, Y., and Prentki, M. (2005) Oleate promotes the proliferation of breast cancer cells via the G protein-coupled receptor GPR40. *J. Biol. Chem.* **280**, 13285–13291
11. Wu, X., Geng, F., Cheng, X., Guo, Q., Zhong, Y., Cloughesy, T. F., *et al.* (2020) Lipid Droplets Maintain Energy homeostasis and glioblastoma growth via Autophagic release of stored fatty acids. *iScience* **23**, 101569
12. Ben-Dror, K., and Birk, R. (2019) Oleic acid ameliorates palmitic acid-induced ER stress and inflammation markers in naive and cerulein-treated exocrine Pancreas Cells. *Biosci. Rep.* **39**, BSR20190054
13. Perez-Marti, A., Ramakrishnan, S., Li, J., Dugourd, A., Molenaar, M. R., De La Motte, L. R., *et al.* (2022) Reducing lipid bilayer stress by monounsaturated fatty acids protects renal proximal tubules in diabetes. *Elife* **11**, e74391
14. Yang, W. S., Kim, K. J., Gaschler, M. M., Patel, M., Shchepinov, M. S., and Stockwell, B. R. (2016) Peroxidation of polyunsaturated fatty acids by lipoxygenases drives ferroptosis. *Proc. Natl. Acad. Sci. U. S. A.* **113**, E4966–E4975

15. Vriens, K., Christen, S., Parik, S., Broekaert, D., Yoshinaga, K., Talebi, A., *et al.* (2019) Evidence for an alternative fatty acid desaturation pathway increasing cancer plasticity. *Nature* **566**, 403–406
16. Magtanong, L., Ko, P. J., To, M., Cao, J. Y., Forcina, G. C., Tarangelo, A., *et al.* (2019) Exogenous monounsaturated fatty acids promote a ferroptosis-resistant cell state cell. *Chem. Biol.* **26**, 420–432.e429
17. Brown, M. S., Radhakrishnan, A., and Goldstein, J. L. (2018) Retrospective on cholesterol homeostasis: the central role of Scap. *Annu. Rev. Biochem.* **87**, 783–807
18. Cheng, X., Li, J., and Guo, D. (2018) SCAP/SREBPs are central Players in lipid metabolism and novel metabolic targets in Cancer Therapy. *Curr. Top. Med. Chem.* **18**, 484–493
19. Guo, D., Prins, R. M., Dang, J., Kuga, D., Iwanami, A., Soto, H., *et al.* (2009) EGFR signaling through an Akt-SREBP-1-dependent, rapamycin-resistant pathway sensitizes glioblastomas to antilipogenic therapy. *Sci. Signal.* **2**, ra82
20. Guo, D., Reinitz, F., Youssef, M., Hong, C., Nathanson, D., Akhavan, D., *et al.* (2011) An LXR agonist promotes glioblastoma cell death through inhibition of an EGFR/AKT/SREBP-1/LDLR-dependent pathway. *Cancer Discov.* **1**, 442–456
21. Cheng, C., Geng, F., Li, Z., Zhong, Y., Wang, H., Cheng, X., *et al.* (2022) Ammonia stimulates SCAP/Insig dissociation and SREBP-1 activation to promote lipogenesis and tumour growth. *Nat. Metab.* **4**, 575–588
22. Li, Y., Wu, S., Zhao, X., Hao, S., Li, F., Wang, Y., *et al.* (2023) Key events in cancer: dysregulation of SREBPs. *Front. Pharmacol.* **14**, 1130747
23. Yang, J., and Stack, M. S. (2020) Lipid regulatory proteins as potential therapeutic targets for ovarian cancer in obese Women. *Cancers (Basel)* **12**, 3469
24. Goldstein, J. L., DeBose-Boyd, R. A., and Brown, M. S. (2006) Protein sensors for membrane sterols. *Cell* **124**, 35–46
25. Nohturfft, A., Yabe, D., Goldstein, J. L., Brown, M. S., and Espenshade, P. J. (2000) Regulated step in cholesterol feedback localized to budding of SCAP from ER membranes. *Cell* **102**, 315–323
26. Sun, L. P., Seemann, J., Goldstein, J. L., and Brown, M. S. (2007) Sterol-regulated transport of SREBPs from endoplasmic reticulum to Golgi: insig renders sorting signal in Scap inaccessible to COPII proteins. *Proc. Natl. Acad. Sci. U. S. A.* **104**, 6519–6526
27. Susman, S., Pirlog, R., Leucuta, D., Mitre, A. O., Padurean, V. A., Melincovici, C., *et al.* (2019) The role of p-Stat3 Y705 immunohistochemistry in glioblastoma prognosis. *Diagn. Pathol.* **14**, 124
28. Heichler, C., Scheibe, K., Schmied, A., Geppert, C. I., Schmid, B., Wirtz, S., *et al.* (2020) STAT3 activation through IL-6/IL-11 in cancer-associated fibroblasts promotes colorectal tumour development and correlates with poor prognosis. *Gut* **69**, 1269–1282
29. Siveen, K. S., Sikka, S., Surana, R., Dai, X., Zhang, J., Kumar, A. P., *et al.* (2014) Targeting the STAT3 signaling pathway in cancer: role of synthetic and natural inhibitors. *Biochim. Biophys. Acta* **1845**, 136–154
30. Mora, L. B., Buettner, R., Seigne, J., Diaz, J., Ahmad, N., Garcia, R., *et al.* (2002) Constitutive activation of Stat3 in human prostate tumors and cell lines: direct inhibition of Stat3 signaling induces apoptosis of prostate cancer cells. *Cancer Res.* **62**, 6659–6666
31. Johnson, D. E., O'Keefe, R. A., and Grandis, J. R. (2018) Targeting the IL-6/JAK/STAT3 signalling axis in cancer. *Nat. Rev. Clin. Oncol.* **15**, 234–248
32. Huynh, J., Chand, A., Gough, D., and Ernst, M. (2019) Therapeutically exploiting STAT3 activity in cancer - using tissue repair as a road map. *Nat. Rev. Cancer* **19**, 82–96
33. Li, Z., Zhu, T., Xu, Y., Wu, C., Chen, J., Ren, Y., *et al.* (2019) A novel STAT3 inhibitor, HJC0152, exerts potent antitumor activity in glioblastoma. *Am. J. Cancer Res.* **9**, 699–713
34. Zhang, X., Yue, P., Page, B. D., Li, T., Zhao, W., Namanja, A. T., *et al.* (2012) Orally bioavailable small-molecule inhibitor of transcription factor Stat3 regresses human breast and lung cancer xenografts. *Proc. Natl. Acad. Sci. U. S. A.* **109**, 9623–9628
35. Bai, L., Zhou, H., Xu, R., Zhao, Y., Chinnaswamy, K., McEachern, D., *et al.* (2019) A potent and selective small-molecule degrader of STAT3 Achieves Complete tumor Regression In Vivo. *Cancer Cell* **36**, 498–511.e417
36. Pajak, B. (2022) Looking for the holy Grail-drug Candidates for glioblastoma multiforme Chemotherapy. *Biomedicines* **10**, 1001
37. Lee, C., and Cheung, S. T. (2019) STAT3: an emerging therapeutic target for hepatocellular carcinoma. *Cancers (Basel)* **11**, 1646
38. Guillou, H., Zadravec, D., Martin, P. G., and Jacobsson, A. (2010) The key roles of elongases and desaturases in mammalian fatty acid metabolism: insights from transgenic mice. *Prog. Lipid Res.* **49**, 186–199
39. Triki, M., Rinaldi, G., Planque, M., Broekaert, D., Winkelkotte, A. M., Maier, C. R., *et al.* (2020) mTOR signaling and SREBP activity increase FADS2 expression and can activate Sapienate biosynthesis. *Cell Rep.* **31**, 107806
40. Bid, H. K., Kibler, A., Phelps, D. A., Manap, S., Xiao, L., Lin, J., *et al.* (2013) Development, characterization, and reversal of acquired resistance to the MEK1 inhibitor selumetinib (AZD6244) in an in vivo model of childhood astrocytoma. *Clin. Cancer Res.* **19**, 6716–6729
41. Jung, K. H., Yoo, W., Stevenson, H. L., Deshpande, D., Shen, H., Gagea, M., *et al.* (2017) Multifunctional effects of a small-molecule STAT3 inhibitor on NASH and Hepatocellular carcinoma in mice. *Clin. Cancer Res.* **23**, 5537–5546
42. Rath, K. S., Naidu, S. K., Lata, P., Bid, H. K., Rivera, B. K., McCann, G. A., *et al.* (2014) HO-3867, a safe STAT3 inhibitor, is selectively cytotoxic to ovarian cancer. *Cancer Res.* **74**, 2316–2327
43. Castro-Mondragon, J. A., Riudavets-Puig, R., Rauluseviciute, I., Lemma, R. B., Turchi, L., Blanc-Mathieu, R., *et al.* (2022) Jaspar 2022: the 9th release of the open-access database of transcription factor binding profiles. *Nucleic Acids Res.* **50**, D165–D173
44. Sandelin, A., Alkema, W., Engstrom, P., Wasserman, W. W., and Lenhard, B. (2004) JASPAR: an open-access database for eukaryotic transcription factor binding profiles. *Nucleic Acids Res.* **32**, D91–D94
45. Bennett, M. K., Lopez, J. M., Sanchez, H. B., and Osborne, T. F. (1995) Sterol regulation of fatty acid synthase promoter. Coordinate feedback regulation of two major lipid pathways. *J. Biol. Chem.* **270**, 25578–25583
46. Jeon, T. I., and Osborne, T. F. (2012) SREBPs: metabolic integrators in physiology and metabolism. *Trends Endocrinol. Metab.* **23**, 65–72
47. Ru, P., Hu, P., Geng, F., Mo, X., Cheng, C., Yoo, J. Y., *et al.* (2017) Feedback Loop regulation of SCAP/SREBP-1 by miR-29 modulates EGFR signaling-Driven glioblastoma growth. *Cell Rep.* **18**, 1076–1077
48. Bao, J., Zhu, L., Zhu, Q., Su, J., Liu, M., and Huang, W. (2016) SREBP-1 is an independent prognostic marker and promotes invasion and migration in breast cancer. *Oncol. Lett.* **12**, 2409–2416
49. Lewis, C. A., Brault, C., Peck, B., Bensaad, K., Griffiths, B., Mitter, R., *et al.* (2015) SREBP maintains lipid biosynthesis and viability of cancer cells under lipid- and oxygen-deprived conditions and defines a gene signature associated with poor survival in glioblastoma multiforme. *Oncogene* **34**, 5128–5140
50. Zou, X. Z., Hao, J. F., and Zhou, X. H. (2021) Inhibition of SREBP-1 activation by a novel small-molecule inhibitor enhances the Sensitivity of Hepatocellular carcinoma tissue to Radiofrequency Ablation. *Front. Oncol.* **11**, 796152
51. Chen, Y. Y., Ge, J. Y., Zhu, S. Y., Shao, Z. M., and Yu, K. D. (2022) Copy number amplification of ENSA promotes the progression of triple-negative breast cancer via cholesterol biosynthesis. *Nat. Commun.* **13**, 791
52. Svensson, R. U., Parker, S. J., Eichner, L. J., Kolar, M. J., Wallace, M., Brun, S. N., *et al.* (2016) Inhibition of acetyl-CoA carboxylase suppresses fatty acid synthesis and tumor growth of non-small-cell lung cancer in preclinical models. *Nat. Med.* **22**, 1108–1119
53. Pizer, E. S., Thupari, J., Han, W. F., Pinn, M. L., Chrest, F. J., Frehywot, G. L., *et al.* (2000) Malonyl-coenzyme-A is a potential mediator of cytotoxicity induced by fatty-acid synthase inhibition in human breast cancer cells and xenografts. *Cancer Res.* **60**, 213–218
54. Shiragami, R., Murata, S., Kosugi, C., Tezuka, T., Yamazaki, M., Hirano, A., *et al.* (2013) Enhanced antitumor activity of cerulenin combined with oxaliplatin in human colon Cancer Cells. *Int. J. Oncol.* **43**, 431–438
55. Liu, Z. L., Wang, G., Shu, Y., Zou, P. A., Zhou, Y., and Yin, Q. S. (2012) Enhanced antitumor activity of epirubicin combined with cerulenin in osteosarcoma. *Mol. Med. Rep.* **5**, 326–330

56. Hu, X., Xiang, J., Li, Y., Xia, Y., Xu, S., Gao, X., *et al.* (2022) Inhibition of stearoyl-CoA desaturase 1 Potentiates anti-tumor activity of Amodiaquine in non-small cell Lung Cancer. *Biol. Pharm. Bull.* **45**, 438–445
57. von Roemeling, C. A., Marlow, L. A., Wei, J. J., Cooper, S. J., Caulfield, T. R., Wu, K., *et al.* (2013) Stearoyl-CoA desaturase 1 is a novel molecular therapeutic target for clear cell renal cell carcinoma. *Clin. Cancer Res.* **19**, 2368–2380
58. Kelly, W., Diaz Duque, A. E., Michalek, J., Konkel, B., Caflisch, L., Chen, Y., *et al.* (2023) Phase II investigation of TVB-2640 (Denifanstat) with Bevacizumab in patients with first Relapse high-grade astrocytoma. *Clin. Cancer Res.* **29**, 2419–2425
59. Falchook, G., Infante, J., Arkenau, H. T., Patel, M. R., Dean, E., Borazanci, E., *et al.* (2021) First-in-human study of the safety, pharmacokinetics, and pharmacodynamics of first-in-class fatty acid synthase inhibitor TVB-2640 alone and with a taxane in advanced tumors. *EClinicalMedicine* **34**, 100797
60. Bergman, A., Carvajal-Gonzalez, S., Tarabar, S., Saxena, A. R., Esler, W. P., and Amin, N. B. (2020) Safety, Tolerability, pharmacokinetics, and pharmacodynamics of a liver-targeting acetyl-CoA carboxylase inhibitor (PF-05221304): a three-Part Randomized phase 1 study. *Clin. Pharmacol. Drug Dev.* **9**, 514–526
61. Calle, R. A., Amin, N. B., Carvajal-Gonzalez, S., Ross, T. T., Bergman, A., Aggarwal, S., *et al.* (2021) ACC inhibitor alone or co-administered with a DGAT2 inhibitor in patients with non-alcoholic fatty liver disease: two parallel, placebo-controlled, randomized phase 2a trials. *Nat. Med.* **27**, 1836–1848
62. Amin, N. B., Darekar, A., Anstee, Q. M., Wong, V. W., Tacke, F., Vourvahis, M., *et al.* (2022) Efficacy and safety of an orally administered DGAT2 inhibitor alone or coadministered with a liver-targeted ACC inhibitor in adults with non-alcoholic steatohepatitis (NASH): rationale and design of the phase II, dose-ranging, dose-finding, randomised, placebo-controlled MIRNA (Metabolic Interventions to Resolve NASH with fibrosis) study. *BMJ Open* **12**, e056159
63. Kamisuki, S., Mao, Q., Abu-Elheiga, L., Gu, Z., Kugimiya, A., Kwon, Y., *et al.* (2009) A small molecule that blocks fat synthesis by inhibiting the activation of SREBP. *Chem. Biol.* **16**, 882–892
64. Gholkar, A. A., Cheung, K., Williams, K. J., Lo, Y. C., Hamideh, S. A., Nnebe, C., *et al.* (2016) Fatostatin Inhibits cancer cell proliferation by affecting Mitotic Microtubule Spindle Assembly and cell Division. *J. Biol. Chem.* **291**, 17001–17008
65. Gyamfi, J., Yeo, J. H., Kwon, D., Min, B. S., Cha, Y. J., Koo, J. S., *et al.* (2021) Interaction between CD36 and FABP4 modulates adipocyte-induced fatty acid import and metabolism in breast cancer. *NPJ Breast Cancer* **7**, 129
66. Rozovski, U., Harris, D. M., Li, P., Liu, Z., Jain, P., Ferrajoli, A., *et al.* (2018) STAT3-activated CD36 facilitates fatty acid uptake in chronic lymphocytic leukemia cells. *Oncotarget* **9**, 21268–21280
67. Sp, N., Kang, D. Y., Kim, D. H., Park, J. H., Lee, H. G., Kim, H. J., *et al.* (2018) Nobiletin Inhibits CD36-dependent tumor Angiogenesis, migration, invasion, and Sphere formation through the Cd36/Stat3/Nf-Kappab signaling Axis. *Nutrients* **10**, 772
68. Zhang, Y., Guo, H., Zhang, Z., Lu, W., Zhu, J., and Shi, J. (2022) IL-6 promotes chemoresistance via upregulating CD36 mediated fatty acids uptake in acute myeloid leukemia. *Exp. Cell Res.* **415**, 113112
69. Ru, P., Hu, P., Geng, F., Mo, X., Cheng, C., Yoo, J. Y., *et al.* (2016) Feedback Loop regulation of SCAP/SREBP-1 by miR-29 modulates EGFR signaling-Driven glioblastoma growth. *Cell Rep.* **16**, 1527–1535
70. Wang, M., and Han, X. (2014) Multidimensional mass spectrometry-based shotgun lipidomics. *Methods Mol. Biol.* **1198**, 203–220
71. Cheng, X., Geng, F., Pan, M., Wu, X., Zhong, Y., Wang, C., *et al.* (2020) Targeting DGAT1 ameliorates glioblastoma by increasing fat Catabolism and Oxidative Stress. *Cell Metab.* **32**, 229–242.e228
72. Han, X., Yang, K., and Gross, R. W. (2008) Microfluidics-based electrospray ionization enhances the intrasource separation of lipid classes and extends identification of individual molecular species through multidimensional mass spectrometry: development of an automated high-throughput platform for shotgun lipidomics. *Rapid Commun. Mass Spectrom.* **22**, 2115–2124
73. Wang, M., Wang, C., Han, R. H., and Han, X. (2016) Novel advances shotgun lipidomics biology medicine. *Prog. Lipid Res.* **61**, 83–108
74. Yang, K., Cheng, H., Gross, R. W., and Han, X. (2009) Automated lipid identification and quantification by multidimensional mass spectrometry-based shotgun lipidomics. *Anal. Chem.* **81**, 4356–4368
75. Cheng, C., Guo, J. Y., Geng, F., Wu, X., Cheng, X., Li, Q., *et al.* (2016) Analysis of SCAP N-glycosylation and trafficking in human cells. *J. Vis. Exp.*, 54709. https://doi.org/10.3791/54709
76. Nohturfft, A., Brown, M. S., and Goldstein, J. L. (1998) Topology of SREBP cleavage-activating protein, a polytopic membrane protein with a sterol-sensing domain. *J. Biol. Chem.* **273**, 17243–17250
77. Pappas, A., Anthonavage, M., and Gordon, J. S. (2002) Metabolic fate and selective utilization of major fatty acids in human sebaceous gland. *J. Invest. Dermatol.* **118**, 164–171
78. Dif, N., Euthine, V., Gonnet, E., Laville, M., Vidal, H., and Lefai, E. (2006) Insulin activates human sterol-regulatory-element-binding protein-1c (SREBP-1c) promoter through SRE motifs. *Biochem. J.* **400**, 179–188